Journal of Zhejiang University-SCIENCE A (Applied Physics & Engineering) in press
www.jzus.zju.edu.cn; www.springer.com/journal/11582
E-mail: jzus_a@zju.edu.cn

Research Article

https://doi.org/10.1631/jzus.A2400357

Thermal-induced upwarp buckling analysis of CRTS II slab ballastless tracks experiencing joint damage

Chang XU[1,2], Tianci XU[1,2], Weixing LIU[1,2], Zhixuan WANG[1,2], Pingrui ZHAO[1,2]✉

[1]*MOE Key Laboratory of High-Speed Railway Line Engineering, Southwest Jiaotong University, Chengdu 610031, China*
[2]*School of Civil Engineering, Southwest Jiaotong University, Chengdu 610031, China*

Abstract: When subjected to sustained high temperatures, the continuous CRTS II railway track structure is susceptible to internal axial pressure, leading to joint damage and the potential for upwarp buckling of the track slab. This study employs model testing to derive the upwarp buckling deformation curve of the slab under conditions of joint damage. An analytical expression for the upwarp buckling equilibrium path of the track slab is derived through the application of the energy principle. Validation of the outcomes is performed by comparison with experimental data. The effects of initial upwarp amplitude, initial upwarp curve type, elastic modulus, thickness, and gravity load on the upwarp buckling response of the track slab were investigated. The results show that: 1) The upwarp deformation of the track slab in the narrow joint damage state is concentrated in a minor range on both sides of the joint, forming an inverted 'V' shape with concave ends. 2) The joint damage can significantly reduce the upwarp buckling critical temperature rise of the track slab. 3) The magnitude of the initial upwarp amplitude dictates the buckling mode of the track slab, while the initial upwarp curve predominantly influences the upwarp buckling critical temperature rise. Notably, an initial upwarp amplitude below 6.5 mm ensures buckling resistance for up to a 60°C temperature rise. 4) Increases in elastic modulus, gravity load, and track slab thickness can increase the upwarp buckling critical temperature rise. As the initial upwarp amplitude increases, the influence of these factors on the upwarp buckling critical temperature rise of the track slab gradually diminishes.

Keywords: CRTS II slab track; Joint damage; Upwarp buckling; Deformation energy; Temperature load

1 Introduction

The China Railway Track System (CRTS) II slab ballastless track is one of the main structures used in China 's high-speed railway system. It is comprised of components including the rail, prefabricated track slab, high elastic modulus cement asphalt (CA) mortar, a concrete base, and an auxiliary structure. Longitudinal connectivity of the track slabs is achieved through tensioning locks and concrete in both wide and narrow joints, as shown in Fig. 1. This system is widely used in high-speed railways due to its advantages of integrity, uniformity, and high longitudinal and lateral anti-slip resistance (Li et al., 2023; Matias and Ferreira, 2022). As of 2022, the cumulative mileage of CRTS II slab track is about 10000 km, constituting about 1/4 of the total length of China 's ballastless track lines (Xu, 2022). The strong longitudinal restraint characteristics of the CRTS II track come with an incapacity to dissipate the accumulated temperature forces within the structure, consequently leading to susceptibility to interlayer debonding during prolonged temperature cycles. In addition, the space of concrete pouring at the joint position is narrow, the concrete is difficult to fully vibrate, and the construction quality is difficult to guarantee. During the operation process, these tracks are notably influenced by factors such as temperature, water, and dynamic loads from trains. This often becomes a high-incidence aspect of the upwarping in the CRTS II slab track system. Under exceptionally high temperatures, the joints primarily manifest issues such as compression cracking and joint defects, as shown in Fig. 2 (Dai and Ge, 2020; Shi and Sheng, 2022). On-site investigations have revealed recurrent upwarp issues in longitudinally connected slab tracks

✉ Pingrui ZHAO, przhao@163.com
Chang XU, https://orcid.org/0009-0008-6929-6619

Received July 12, 2024; Revision accepted Dec. 19, 2024; Crosschecked

during long-term high-temperature conditions in summer. The maximum upwarp amplitude can reach tens of millimeters, significantly compromising the structural performance and impeding the high-speed operation of trains (Zhao et al., 2017).

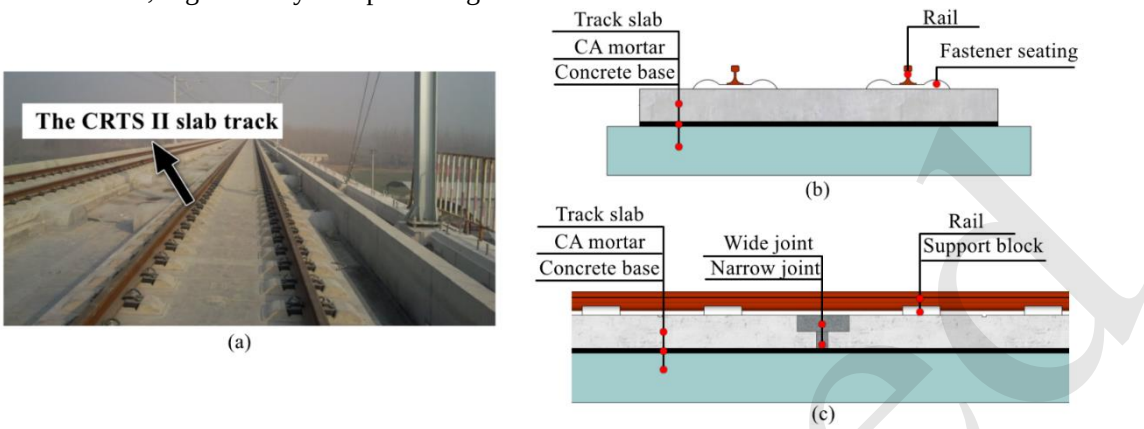

Fig. 1 The structure of CRTS II slab track: (a) site photograph; (b) front view; (c) side view

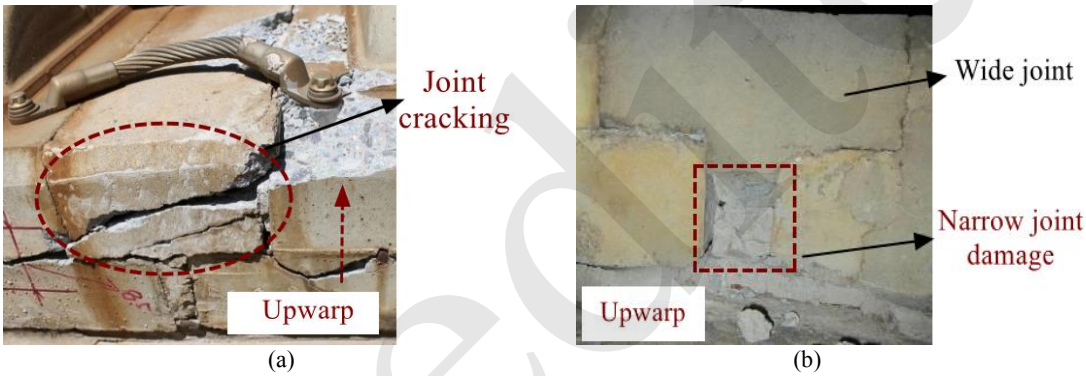

Fig. 2 Typical joint damage: (a) compression cracking; (b) defect and falling block

Presently, the primary emphasis in research on CRTS II slab ballastless tracks revolves around the evolution of structural damage, measures for upwarp prevention, and the vertical stability of the track slab. Cai et al. (2019), Liu et al. (2019), and Huang et al. (2021) reproduced the damage development process of wide and narrow joints in a high temperature environment by establishing a three-dimensional finite element model, and clarified that the arching is mainly related to the eccentric compression caused by joint damage. Zhong et al. (2018) and Zhang et al. (2022) undertook prolonged monitoring of the temperature field in CRTS II slab tracks, delving into the temperature distribution characteristics of the track structure and the time-varying characteristics of the temperature effects. Zhou et al. (2024) employed a combination of indoor experiments and thermal-mechanical coupling simulations to elucidate the dynamic response behavior of the longitudinal track structure under the combined effects of temperature and moving train loads, and found that temperature load plays a more important role in the coupling effect. Song et al. (2020) proposed an analysis method for thermal deformation and interface separation in CRTS II slab track structures, and revealed the evolution process and vulnerable areas prone to interlayer damage. Lou et al. (2023) accounted for the impact of the service environment on the arching and interlayer failure of a track, elucidating the deformation characteristics of CRTS II slab track in high altitude climates. Zhou et al. (2022; 2023) conducted a large-scale model test on CRTS II slab track, obtaining the temperature distribution and stress response of the track structure under continuous daytime high temperature conditions. Various three-dimensional nonlinear models were employed to investigate the damage evolution characteristics of wide and narrow joints, as

well as interlayer interfaces.

In the realm of track slab upwarp prevention and control, Ma et al. (2024) introduced an efficient method for track arching identification based on deep learning and dynamic detection data, enabling precise and rapid detection of arching with a gap height exceeding 1 mm. Tang et al. (2023) investigated the impact zone of track arching on vehicle acceleration and developed a cost-effective arching recognition method utilizing convolutional neural networks and vehicle responses. Li et al. (2021; 2023) investigated the arch deformation and structural damage characteristics of longitudinal slab tracks under extreme heat waves, simulating the high temperature arching phenomenon of the track system following the installation of anchor bars. The results indicated that reinforcement with embedded steel bars effectively mitigates arch displacement in the track slab induced by temperature increases. Additionally, Xu et al. (2020) and Yan et al. (2023) used an improved cohesion model to evaluate the effect of interlayer debonding repair on the interface damage and thermal deformation of CRTS II slab track. Their results showed that debonding repair continues to exhibit a positive reparative effect even under extreme temperature conditions. Moreover, He et al. (2024) proposed a new elastic T-joint designed to mitigate damage to the joints and interlayer interfaces of the longitudinal slab track structure in extreme high temperature environments, and studied the effects of the size, material properties, and replacement position of the elastic joint on the track damage, deformation, and mechanical properties.

Investigations into the longitudinal track structure's upwarp stability predominantly employ theoretical derivations. For example, Yang et al. (2015) introduced a formula for calculating the critical temperature force of CRTS II track slab by referring to the equal wavelength model in continuous welded rail (CWR). Zhang et al. (2020) simplified the track slab into an elastic thin plate and derived a formula for the upwarp stability under varied interlayer conditions. Through the application of the unequal wavelength model, Chen et al. (2018) elucidated the relationship between temperature rise and upwarp amplitude of the track slab. Also, Liu (2018) explored the deformation waveform of the track slab in an ideal state, employing differential equations to examine the effects of various factors on the slab's equilibrium path. Furthermore, Chen et al. (2023) studied the influence of the stiffness of the wide and narrow joints on the track slab stability, and concluded that reducing the joint stiffness is an effective way to improve the track slab stability. Xu et al. (2021) presented an analytical solution for track slab arching through differential equation resolution, probing the effects of CA mortar bond softening on the buckling of the track slab. Zhang (2021) utilized theoretical and analytical methods to investigate the longitudinal and vertical interface behavior and damage mechanisms between layers of longitudinally connected slab tracks under temperature loads. This clarified the influence of interface parameters, such as bonding strength and stiffness, on interface damage.

Although a large number of scholars have studied the thermal-induced upwarp issue of CRTS II slab track, the following deficiencies still exist: a) Current research tends to adopt an oversimplified approach by modeling the track slab as a uniform two-dimensional Euler beam, deriving the upwarp curve through assumed deformations or differential equation solutions. This simplification overlooks the longitudinal non-uniformity of the track slab, and therefore fails to accurately capture the deformation characteristics of the track slab during unstable stages. b) Theoretical derivations address joint damage through stiffness degradation at specific locations, an approach that inadequately represents the comprehensive impact of joint defects on track slab stability. c) Simulation analyses primarily concentrate on interface failure and material damage evolution within the track structure under loading, neglecting the upwarp equilibrium development path of the track slab under the joint damage state. Consequently, there is a pronounced need for further exploration into the thermal-induced upwarp buckling of CRTS II slab tracks under joint damage.

In this study, we first conduct model tests of the upwarp buckling of the track slab, with a comparative analysis of the buckling deformation characteristics of the track slab under intact conditions and narrow joint defect conditions. Subsequently, by leveraging the energy method in conjunction with the equal wavelength model, the upwarp buckling equilibrium path of the track slab is obtained. Finally, we analyze the impact of the slab's initial state and varying structural parameters on its upwarp buckling behavior.

2 Experiment and methods

2.1 Model and equipment preparation

In field conditions, there are different degrees of damage at the narrow joints of the track slab, and the boundary constraint state of the upwarp section is complex and variable; however, the upwarp range of the track slab generally does not exceed two slabs (Chen et al., 2023). Considering the test fixture, model making, and loading control, the approximate size ratio of the track slab model is set at 1:20 and the model length must be greater than 1300 mm (the length of two track slab models). An aluminum plate measuring 2000 mm × 120 mm × 10 mm (length × width × thickness), characterized by excellent elasticity, ease of processing, and uniformity, is selected to simulate the track slab. A 5 mm horizontal through-cut is introduced at the lower midpoint of the aluminum plate to replicate the most unfavorable damage scenario along the horizontal seam, thereby effectively reproducing the upwarp instability phenomenon of the track slab during testing. The primary parameters of the model are delineated in Table 1.

In the track slab upwarp buckling model test, the first step is to level the experimental device, after which the track slab model is installed within the rectangular groove of the device shown in Fig. 3. To ensure that the slab is in place, a wedge structure is placed at both ends of the device to ensure the constraints of the model. A longitudinal force is applied by the hydraulic jack to simulate the thermal load of the track slab. Throughout the experiment, the upwarp displacement of the track slab model is meticulously monitored in real-time using eight dial indicators. This arrangement allows for the accurate depiction of the upwarp buckling waveform of the track slab, based on the vertical displacement data recorded at each measurement point. The experimental setup is shown in Fig. 4.

2.2 Characteristics of the upwarp buckling deformation of the track slab

Two tests are conducted on both the intact track slab model and the model featuring a narrow joint defect, allowing us to obtain the upwarp buckling deformation of the track slab under varying conditions. To enhance the measurement accuracy, the vertical displacement distribution of the model is measured in the post-buckling stage, after the track slab model reaches the upwarp buckling critical force, as shown in Fig. 5.

Fig. 5(a) reveals that in the absence of joint damage, the upwarp displacement of the track slab incrementally ascends from both extremities towards the middle, with a minor difference in displacement among measuring points near the middle of the slab. This manifests as a deformation pattern characterized by a pronounced upwarp in the middle and diminishment at both ends, forming a symmetrical convex profile. The upwarp buckling deformation of the intact track slab can be succinctly represented by Eq. (1). As shown in Fig. 5(b), in the presence of a narrow

Table 1 Track slab model parameters

Material	Size (length × width × thickness) (mm)	Elastic modulus (MPa)	Density (kg/m^3)	Thermal expansion Coefficient (□$^{-1}$)
Aluminum	2000 × 120 × 10	6.9×10^4	2700	2.35×10^{-5}

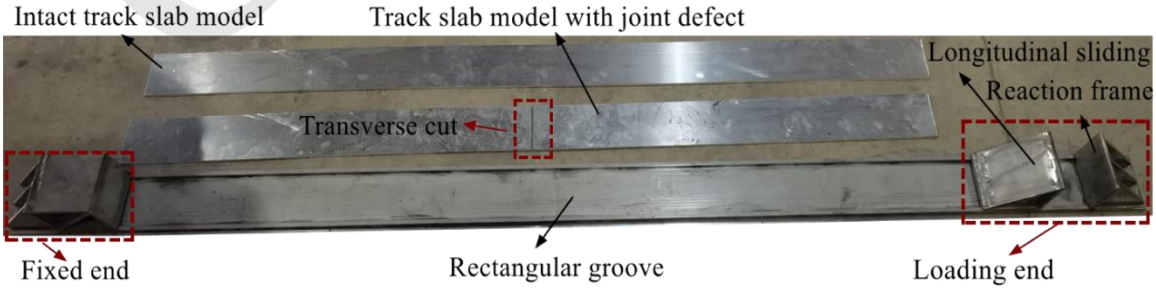

Fig. 3 Test device

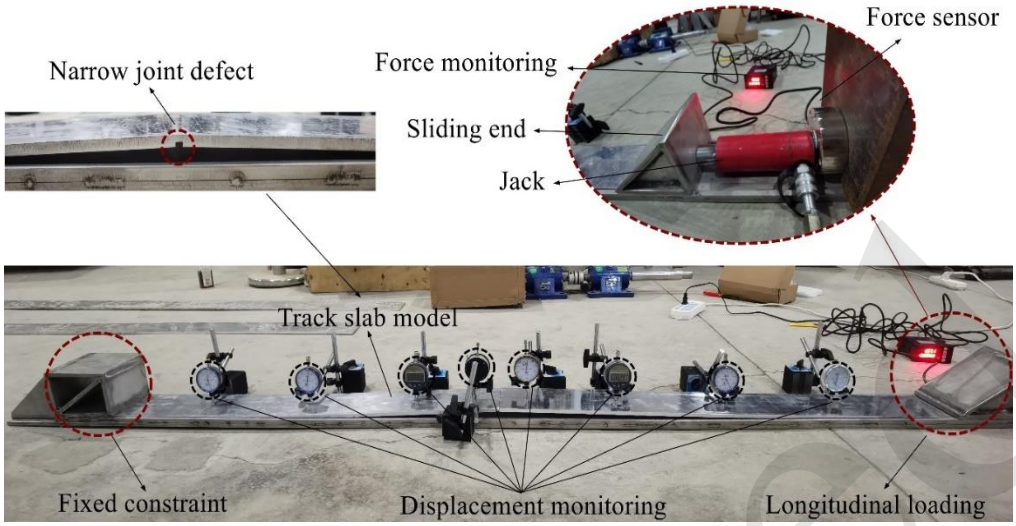

Fig. 4 Experimental testing

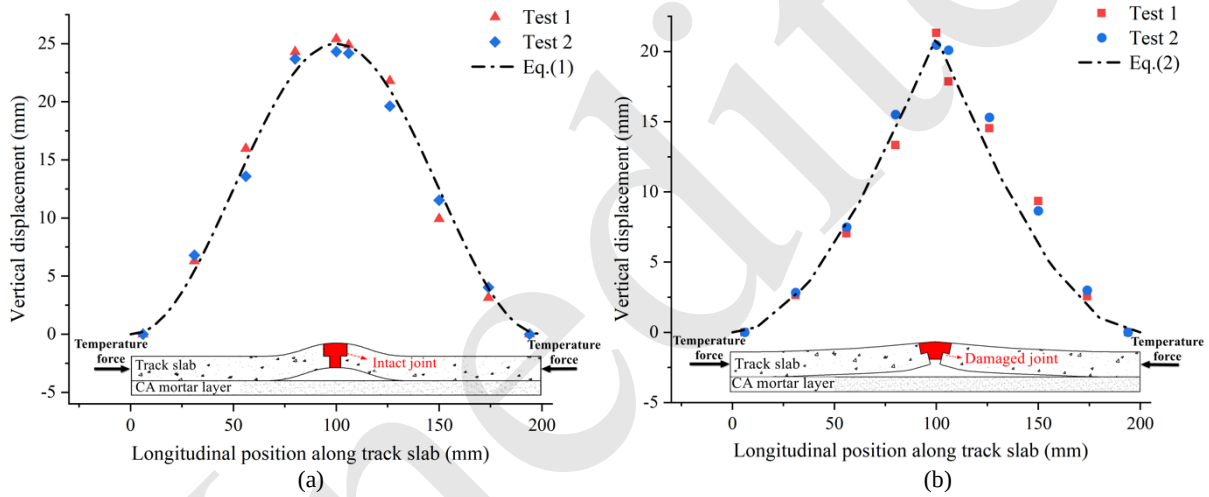

Fig. 5 Vertical displacement of the track slab model: (a) intact track slab model; (b) track slab model with a narrow joint defect

joint defect, the deformation curve of the track slab exhibits a more gradual boundary. The upwarp displacement exhibits minimal variation near the slab's ends, increasing progressively moving closer to the middle, and culminating at its maximum at the site of the joint defect, thereby presenting a generally concave, inverted 'V'-shaped deformation trend. In this case, the upwarp buckling deformation of the track slab can be expressed by Eq. (2). Additionally, because the right side of the model is the loading end, in contrast to the fixed constraint on the left, the end constraint demonstrates relative weakness, leading to a certain deviation in the displacement data of the track slab on the right side of the joint from the fitted curve. A comparison between the upwarp buckling curves of both cases reveals the significant role of the narrow joint defect in defect guiding and diminishing the stiffness of the track slab during upwarping. The track slab with a narrow joint defect is in an eccentric compression state during the upwarping process, resulting in the rotation of the track slab around the joint position. In this way, the bending deformation is more likely to be concentrated near the joint, thus further reducing the bending deformation and upwarp height of the track slab on both sides of the joint.

$$f_1(x) = f_1 \sin^2\left(\frac{\pi x}{l_1}\right), \tag{1}$$

$$f_2(x)=\begin{cases} f_2\left(1-\cos\dfrac{\pi x}{l_2}\right) & 0\le x<\dfrac{l_2}{2} \\ f_2\left(1+\cos\dfrac{\pi x}{l_2}\right) & \dfrac{l_2}{2}\le x\le l_2 \end{cases}, \qquad (2)$$

In these equations, f_1 and l_1 are the maximum upwarp amplitude and upwarp wavelength of the intact track slab model; and f_2 and l_2 are the maximum upwarp amplitude and upwarp wavelength of the track slab model with a narrow joint defect, respectively.

3 Theoretical analysis

3.1 Basic assumptions

To abstract an appropriate mechanical model that simplifies the analysis of upwarp stability of the track slab, maintain computational precision, and account for the structural characteristics of CRTS II slab track, the following basic assumptions are made in this study. The solution process for the theoretical analysis is illustrated in Fig. 6.

(1) Ignoring the lateral influence of the track structure, the longitudinal track slab is regarded as a uniform two-dimensional plane beam with fixed constraints at both ends. Its upwarp at high temperature is within the elastic range of the material, and the nonlinear mechanical properties of the concrete material and the compression failure of the track slab are not considered (Liu, 2023; Zhang, 2021).

(2) It is assumed that the upwarp wavelength at the final buckling is equal to the initial upwarp wavelength of the track slab. And considering that the camber of the track slab involves small deformations, the release of temperature forces during the upwarp process can be neglected (Liu, 2019).

(3) Considering the joint damage of the track slab, the influence of the narrow joint defect is characterized by the change of the upwarp buckling waveform of the track slab.

(4) The 'V'-type cracking on the track slab is only a detailed structure, and the bending resistance of the rail and fastener system is much smaller than that of the track slab itself (Yang et al., 2015). Therefore, the influence of 'V'-type cracking of the rail and fastener system is not considered.

(5) In a long-term operation process, the interlayer bonding between the track slab and the CA mortar is greatly reduced, and there are many interlayer gaps before the upwarping (Chen et al., 2018). Therefore, the bonding effect of the mortar layer on the track slab is not considered.

(6) Concrete creep is a long-term process. The effects of concrete creep and shrinkage on the longitudinal temperature forces experienced by the track slab can be disregarded during the short-term high temperature upwarp (Bouras and Vrcelj, 2020; Liu et al., 2020).

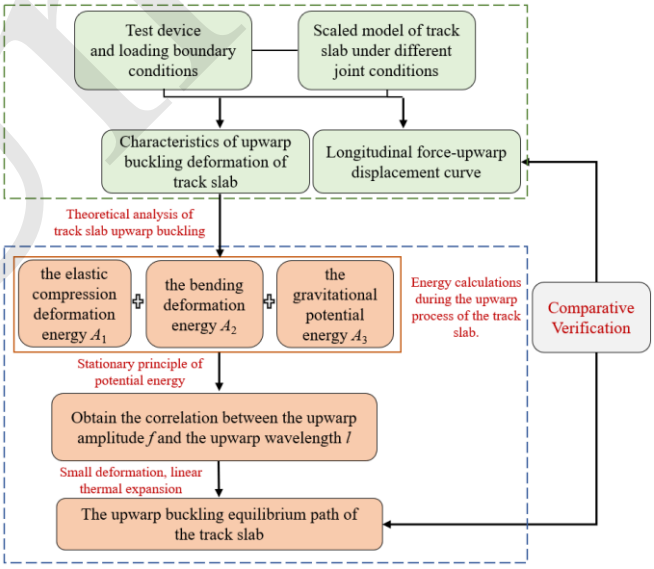

Fig. 6 Calculation workflow used in this study

3.2 Energy method

Before track slab upwarp, the slab may exhibit varying degrees of initial deformation, attributable to factors including manufacturing errors, inaccuracies during laying, foundation deformation during long-term service, train loads, and environmental impact. Currently, it is difficult to obtain the initial upwarp deformation curve of the track slab. Considering that the curvature of the deformed track slab does not change abruptly at the boundary of the upwarp section, we adopt the upwarp buckling curve of the intact track slab as the initial upwarp deformation, which can be expressed as:

$$y_0 = f_0 \sin^2\left(\frac{\pi x}{l}\right), \tag{3}$$

where f_0 and l are the maximum initial upwarp amplitude and upwarp wavelength of the track slab, respectively.

It can be seen from Section 2.2 that the high temperature upwarp deformation curve of the track slab under the condition of narrow joint defect can be expressed as:

$$y = \begin{cases} f\left(1-\cos\dfrac{\pi x}{l}\right) & 0 \le x < \dfrac{l}{2} \\ f\left(1+\cos\dfrac{\pi x}{l}\right) & \dfrac{l}{2} \le x \le l \end{cases}, \tag{4}$$

where f is the maximum upwarp amplitude of the track slab.

The upwarp deformation of the track slab is shown in Fig. 7, and the final deformation curve is given by Eq. (5):

$$y_T = y_0 + y, \tag{5}$$

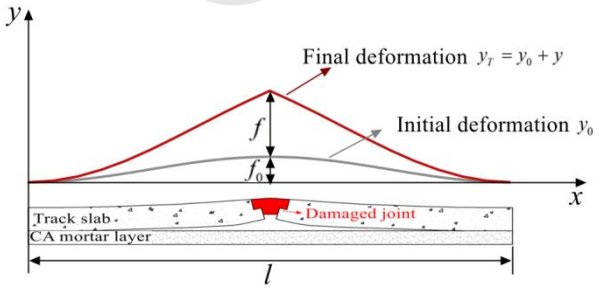

Fig. 7 Upwarp deformation of a track slab

As the overall temperature of the track slab increase, the vertical deformation of the track slab gradually increases until it reaches the buckling state. Throughout this progression, the accumulated total potential energy A of the track slab is mainly composed of three parts: the elastic compression deformation energy A_1 of the track slab, the bending deformation energy A_2, and the gravitational potential energy A_3 of the track slab. Thus we have:

$$A = A_1 + A_2 + A_3, \tag{6}$$

Considering the symmetry of the structure, the half-body structure of the track slab is analyzed, and the compressive deformation energy A_1 of the track slab can be expressed as:

$$A_1 = -P \cdot \Delta l, \tag{7}$$

where P is the longitudinal temperature force in the track slab, and Δl is the axial compression deformation of the track slab caused by the temperature force.

According to the geometric relationship of the change of the arc length before and after track slab upwarp shown in Fig. 8, Δl can be expressed as follows:

$$\Delta l = \int_0^l \left(dl_T - dl_0\right) = \int_0^{\frac{l}{2}} y_T'^2 dx - \int_0^{\frac{l}{2}} y_0'^2 dx, \tag{8}$$

where dl_0 and dl_T are the small arc lengths before and after track slab upwarp, respectively.

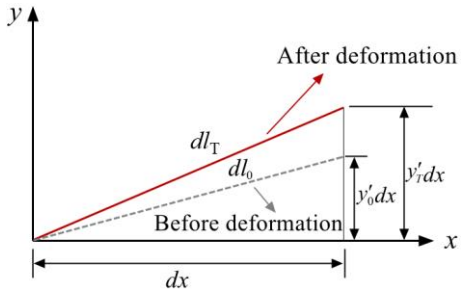

Fig. 8 Differences in the arc length of the track slabs before and after upwarp

Combining Eqs. (7) and (8), the compressional deformation energy A_1 of the track slab can be written as:

$$A_1 = -\frac{P\pi f(16 f_0 + 3\pi f)}{12l} \tag{9}$$

The bending deformation energy A_2 of the track slab can be expressed as:

$$A_2 = 2\times\left(\frac{1}{2}\int_0^{\frac{l}{2}} M d\theta\right) = \int_0^{\frac{l}{2}} EIy''^2 dx = \frac{EIf^2\pi^4}{4l^3} \tag{10}$$

where E is the elastic modulus of the track slab, and I is the cross-sectional moment of inertia of the track slab.

During the upwarping process of the track slab, the gravitational potential energy will continue to increase. The gravitational effect of the track slab is simplified into a uniformly distributed vertical load along its longitudinal axis, and the gravitational potential energy A_3 of track slab is given by:

$$A_3 = 2\times\int_0^{\frac{l}{2}} qy dx = \frac{qfl(\pi-2)}{\pi} \tag{11}$$

where q is the gravity load per unit length of the track slab, $q=\rho A_0 g$; ρ is the density of the track slab; and A_0 is the cross-sectional area of the track slab.

According to the stationary principle of potential energy, the equilibrium condition of the track slab in the process of upwarping is:

$$dA = \frac{\partial A}{\partial f} df + \frac{\partial A}{\partial l} dl = 0 \tag{12}$$

Since df and dl are non-zero arbitrary small quantities, it follows that:

$$\frac{\partial A}{\partial f} = \frac{\partial A}{\partial l} = 0 \tag{13}$$

According to Eq. (13), the relationship between the upwarp amplitude f and the upwarp wavelength l can be obtained.

If the linear expansion coefficient of the concrete material is α, the relationship between the temperature rise amplitude ΔT of the track slab and the theoretical longitudinal temperature force P_t can be written as:

$$\Delta T = \frac{p_t}{\alpha EA} \tag{14}$$

The upwarp buckling of the track slab is a small vertical deformation, and the release of the temperature force caused by the track slab upwarp can be ignored, that is, $P=P_t$. Combined with Eqs. (13) and (14), the corresponding relationship between equivalent temperature rise ΔT and upwarp amplitude f can be obtained by using numerical methods.

3.3 Theoretical verification

The upwarp of the longitudinal track slab is unpredictable and sudden, making field tests difficult. Therefore, the theoretical solution of the upwarp buckling equilibrium path of the track slab model is compared with the experimental results, as shown in Fig. 9. The track slab model is straightened by a straightening machine, and the initial upwarp amplitude f_0 = 1 mm is used in the theoretical calculation. It can be seen from Fig. 9 that the development trend of the upwarp buckling path of the track slab obtained by the theoretical method is close to the test results. Nonetheless, due to the indeterminate initial upwarp curve form and upwarp height of the track slab model, differences exist between the theoretical results and test curves. The upwarp buckling critical loads of the track slab obtained from the two tests are 5 kN and 5.3 kN, respectively. The critical load obtained by theoretical calculation is 4.8 kN, and the relative errors are 4.2% and 10.4%, respectively. In general, the theoretical results are in good agreement with the experimental results, and the relative error is within an acceptable range, helping validate the theoretical method in this paper.

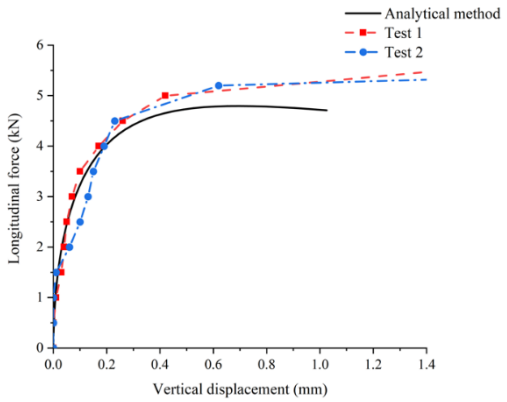

Fig. 9 Comparative verification of the upwarp buckling equilibrium path

4 Results and discussion

4.1 Analysis of the upwarp buckling characteristics of the track slab

Taking the initial upwarp amplitude f_0 = 1 mm of the track slab as an example, the upwarp buckling equilibrium path of the track slab without damage and narrow joint defect, and the variation law of the upwarp amplitude f with the upwarp wavelength l are calculated. The results are shown in Fig. 10 and Fig. 11. The structural parameters of the track slab are shown in Table 2.

It can be seen from Fig. 10 that the upwarp buckling process of the track slab can be divided into three stages. In the initial stage, where the temperature rise is comparatively low, gravitational effects predominate, resulting in negligible variations in the upwarp amplitude in response to temperature rise increases; this is the stable stage of the track slab.

Table 2 Structural parameters of the track slab

Components	Size (width × thickness) (m)	Elastic modulus (MPa)	Density (kg/m^3)	Thermal expansion coefficient (℃$^{-1}$)
Track slab	2.55×0.2	3.55×10^4	2500	1×10^{-5}

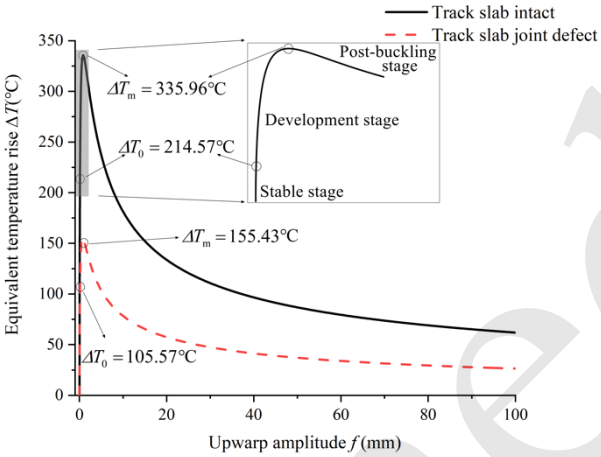

Fig. 10 The upwarp buckling equilibrium path of the track slab

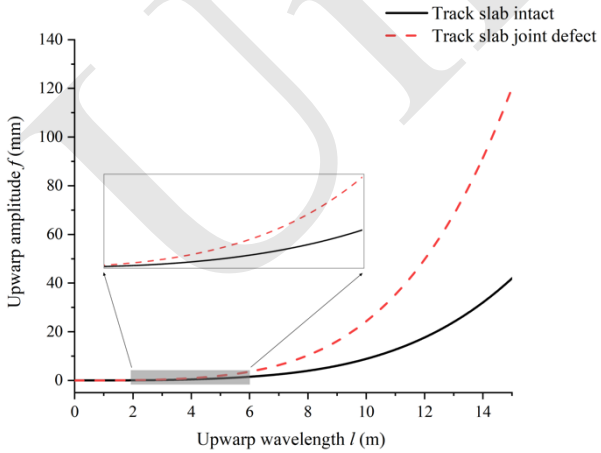

Fig. 11 Variation of upwarp amplitude f with upwarp wavelength l

When the temperature rise reaches ΔT_0, the upwarp amplitude changes significantly with the increase of the temperature rise until it reaches the upwarp buckling critical temperature rise ΔT_m, which is the upwarp development stage of the track slab. When the temperature rise exceeds ΔT_m, the upwarp buckling equilibrium path enters the descending stage, and the equivalent temperature rise decreases rapidly with the increase of the upwarp amplitude and finally trends towards stability, which indicates that the temperature force in the track slab begins to release rapidly. At this time, the track slab enters the post-buckling stage. Compared with the upwarp buckling equilibrium path of the intact track slab, when the track slab reaches the identical upwarp amplitude, the temperature rise required by the track slab with a narrow joint defect is lower, and the upwarp temperature rise ΔT_0 and the upwarp buckling critical temperature rise ΔT_m are significantly reduced. The ΔT_m decreases from 335.96 ℃ to 155.43 ℃, which is only 46.3% of that in the absence of damage. It is evident that the narrow joint defect significantly increases the probability of upwarp buckling of the track slab.

From Fig. 11, it is observable that when the upwarp wavelength of the track slab is less than 2 m, the change in upwarp amplitude remains insignificant. As the upwarp wavelength increases, the rate of increase in upwarp amplitude goes up correspondingly. Regardless of the presence or absence of the joint defect, the upwarp amplitude increases exponentially with the increase of the upwarp wavelength. At an identical upwarp wavelength, the upwarp amplitude of the track slab with a narrow joint defect is

larger, with the difference between the two conditions escalating as the wavelength increases. Conversely, at an identical upwarp amplitude, the upwarp wavelength of the intact track slab is longer, which indicates that the upwarp deformation of the track slab with a narrow joint defect is mainly concentrated in a minor range near the joint.

4.2 The effect of initial upwarp amplitude

According to relevant research on structural stability, the initial imperfection can determine the deformation amplitude and development mode of structural buckling to a certain extent, as it is the key factor leading to structural buckling (Liu, 2019). Existing data indicate that the maximum upwarp amplitude of the on-site track structure does not exceed 50 mm. Therefore, we take the initial upwarp amplitudes as 1 mm, 2 mm, 5 mm, 20 mm, and 50 mm, respectively, in order to study the influence of different initial upwarp amplitudes on the upwarp buckling development of the track slab.

Fig. 12(a) illustrates that the upwarp buckling equilibrium path of the track slab is significantly influenced by the initial upwarp amplitude. When the initial upwarp amplitude is small, the temperature rise increases sharply with the upwarp amplitude, resulting in a minor upwarp buckling critical amplitude; this makes 'sudden buckling' more likely to occur. Conversely, a larger initial upwarp amplitude results in a more gradual temperature rise with the upwarp amplitude of the track slab, extending the upwarp development stage. This prolongation allows for a continued increase in upwarp deformation, transitioning into a 'progressive buckling' mode. The main reason for this behavior, as depicted in Fig. 12(b), is that the initial upwarp amplitude alters the equilibrium state during the upwarping process of the track slab. The larger the initial upwarp amplitude and the larger the vertical component of the longitudinal temperature force, the shorter the upwarp wavelength required for the track slab to reach the identical upwarp amplitude, and the less work needed to overcome gravity, so the equivalent temperature rise is also reduced. As upwarp amplitude increases, the impact of initial upwarp amplitude progressively decreases, leading to a diminishing difference in temperature rise required for identical upwarp amplitudes. Therefore, when the track slab enters the post-buckling stage, the equilibrium path of the track slab with initial upwarping will eventually tend to the equilibrium path without initial upwarping.

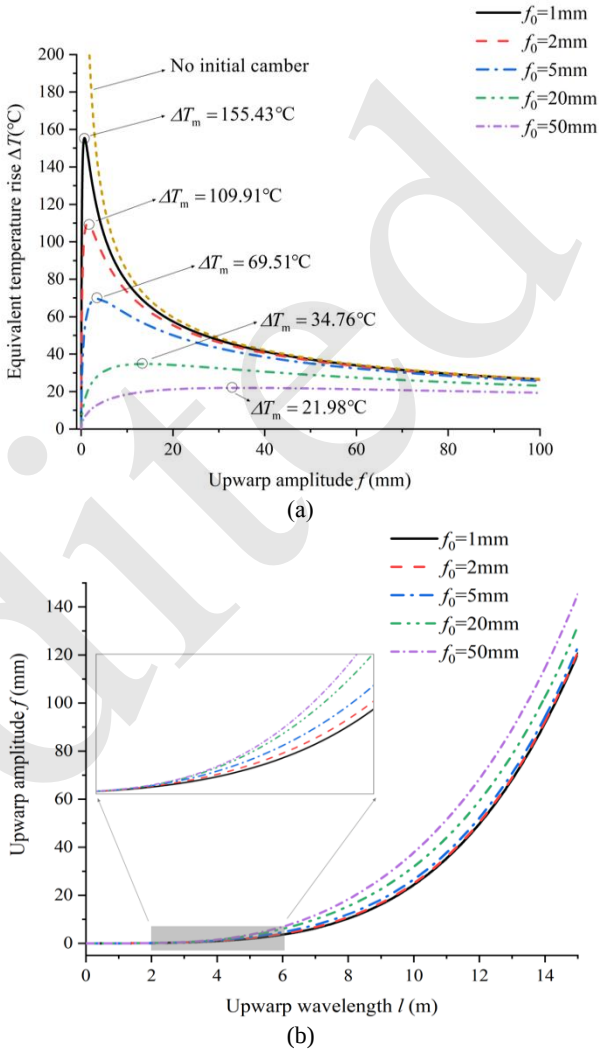

Fig. 12 Effect of f_0 on the upwarp buckling of track slab: (a) upwarp buckling equilibrium path of track slab; (b) variation of upwarp amplitude f with camber wavelength l

The upwarp buckling critical temperature rise of the track slab demonstrates a nonlinear decrease as the initial upwarp amplitude increases. This relationship can be adequately described by a logarithmic function, as shown in Fig. 13. Given that the observed temperature rise within track structures in extremely high temperature environments typically does not exceed 60 ℃, it is advisable to control the initial upwarp amplitude f_0 to not exceed 6.5 mm, in order to prevent buckling of the track slab (Chen et al., 2023).

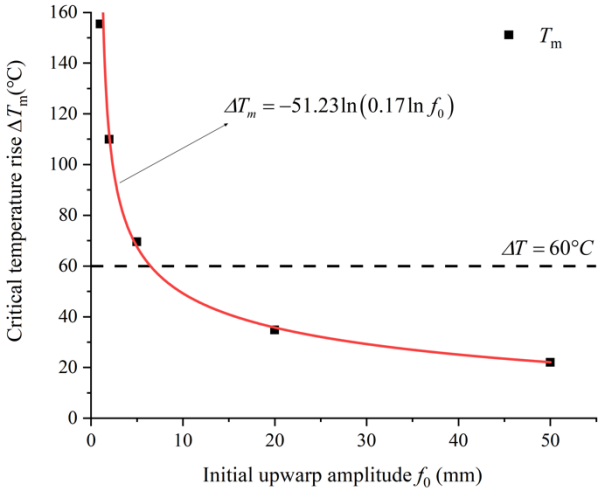

Fig. 13 Variation of ΔT_m with f_0

4.3 The effect of the initial upwarp curve

The initial deformation of the track slab is affected by many factors in the field, and there is no definite curve form. In order to study the thermal-induced upwarp buckling law of the track slab under different initial upwarp curves, we take f_0 = 1 mm as an example, and assume five initial deformation curves of the track slab as shown in Fig. 14. Among them, No.1 and No.2 represent convex deformations, and No.4 and No.5 feature overall concave deformations. The expressions of the four curves are shown in Eqs. (15)-(18), and No.3 is shown in Eq. (3).

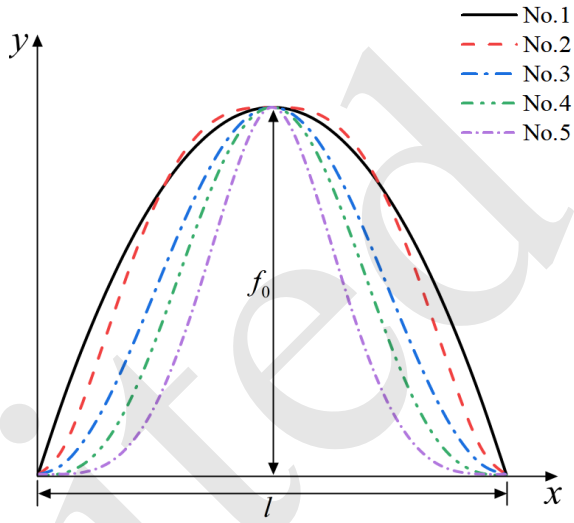

Fig. 14 Different initial upwarp curves of the track slab

$$y_1 = \frac{4f_0x(l-x)}{l^2} \quad 0 \le x \le l, \tag{15}$$

$$y_2 = \begin{cases} f_0\left(1+\frac{5}{2}\left(\frac{2x}{l}-1\right)^3-\frac{3}{2}\left(\frac{2x}{l}-1\right)^5\right) & 0 \le x < l/2 \\ f_0\left(1-\frac{5}{2}\left(\frac{2x}{l}-1\right)^3+\frac{3}{2}\left(\frac{2x}{l}-1\right)^5\right) & l/2 \le x \le l \end{cases}, \tag{16}$$

$$y_4 = f_0\left(0.707-0.2617\left(\frac{\pi x}{l}-\frac{\pi}{2}\right)^2+0.293\cos\left(\frac{2.86\pi x}{l}-1.43\pi\right)\right) \quad 0 \le x \le l, \tag{17}$$

$$y_5 = \begin{cases} -f_0\left(\frac{8x}{l}-5\right)\left(\frac{2x}{l}\right)^4 & 0 \le x < l/2 \\ f_0\left(\frac{8x}{l}-3\right)\left(\frac{2x}{l}-2\right)^4 & l/2 \le x \le l \end{cases}, \tag{18}$$

As shown in Fig. 15(a), a more convex initial upwarp curve results in a smaller upwarp amplitude for the track slab under identical temperature rise load, thereby enhancing its stability. Nevertheless, the

impact of the initial upwarp curve on the upwarp buckling path is predominantly confined to minor upwarp amplitudes. It can be seen from Fig. 15(b) that the upwarp amplitude of the track slab under various initial upwarp curves varies little with the upwarp wavelength. When the upwarp amplitude is 2 mm, the upwarp wavelengths for curves No.1~ No. 5 are 5.15 m, 5.11 m, 5.05 m, 5.01 m, and 5.03 m, respectively. This demonstrates that the initial upwarp curve has negligible influence on the relationship between *f* and *l*, and it primarily affects the upwarp buckling critical temperature rise of the track slab.

This is because different initial upwarp curves impose varying constraints on the track slab upwarping behavior. The more pronounced a concave curve is (with smoother boundaries and a more significant curvature change from end to center), the stronger the constraint exerted at the end of the curve, and the greater the impact on the upwarping behavior of the track slab. Under axial compression, curves with strong end constraints (No.4 and No.5) exhibit a noticeable suppression of upwarping at the slab ends, within a certain range. Therefore, the axial temperature force will force the initially convex part of the track slab to produce a larger upwarp amplitude. This leads to a reduction in the upwarp wavelength for a given upwarp amplitude, which in turn results in a lower upwarp buckling critical temperature rise.

The variation of the upwarp buckling critical temperature rise of the track slab with the initial upwarp curve and the initial upwarp amplitude is shown in Fig. 16. It is clear that as the boundary constraint of the initial upwarp curve gradually enhanced, the impact of increasing initial upwarp amplitude on reducing the critical temperature rise diminishes. When the initial upwarp amplitude is small, the ΔT_m changes significantly with different initial upwarp curves. However, as the initial upwarp amplitude increases, the influence exerted by the initial upwarp curve on ΔT_m gradually weakens. Consequently, the larger the initial upwarp amplitude of the curve and the smoother its boundary, the more susceptible the track slab is to upwarp buckling.

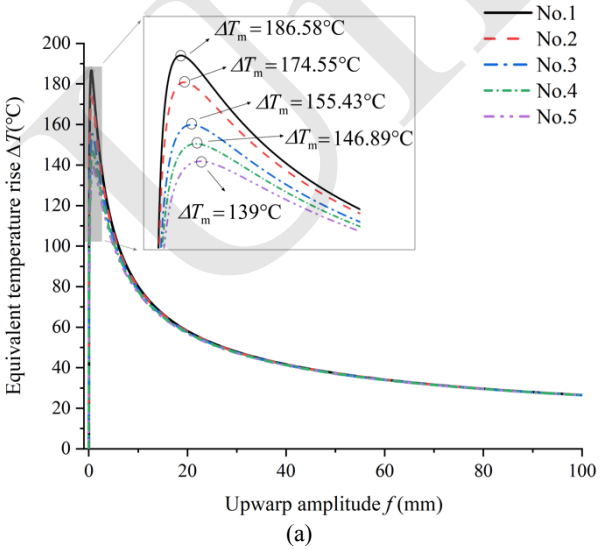

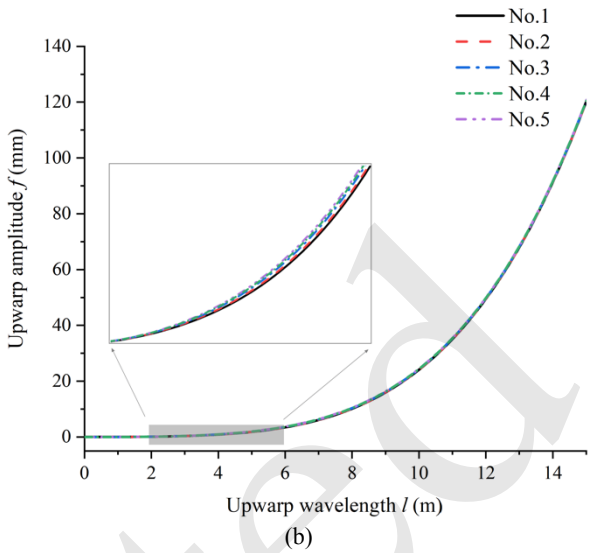

Fig. 15 Effect of the initial upwarp curve on the upwarp buckling of track slab: (a) upwarp buckling equilibrium path of the track slab; (b) variation of upwarp amplitude *f* with camber wavelength *l*

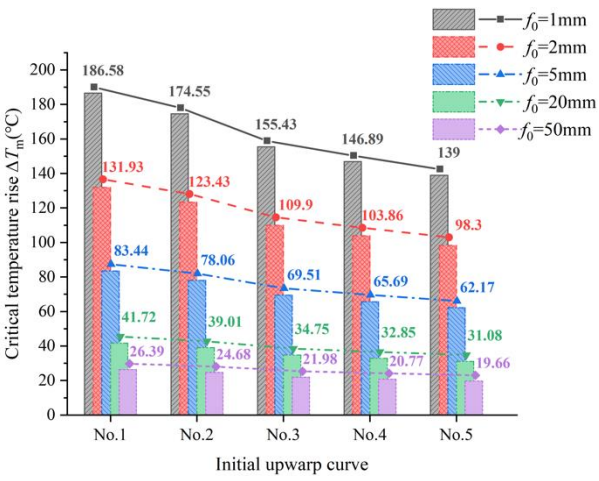

Fig. 16 Variation of ΔT_m with the initial upwarp curve

4.4 The effect of the elastic modulus of the track slab

In order to study the influence of the elastic modulus E of the track slab on its upwarp buckling, we take the initial upwarp curve of No.3 and f_0 = 1 mm as an example, and the concrete grades C30, C40, C55, C70, and C80 are chosen to represent the track slab material, with corresponding elastic moduli of 30.0 GPa, 32.5 GPa, 35.5 GPa, 37.0 GPa, and 38.0 GPa, respectively (Ministry of Housing and Urban-Rural Development of the People's Republic of China, 2015). As shown in Fig. 17(a), the elastic modulus increases, extending the stability stage of the track slab and gradually increasing the upwarp buckling critical temperature rise; in contrast, the upwarp buckling critical amplitude increases only slightly. The elastic modulus has a great influence on the post-buckling behavior of the track slab. Observations from Fig. 17(b) reveal that the increase of the track slab's elastic modulus makes the upwarp wavelength gradually increase under an identical upwarp amplitude, and the larger the upwarp amplitude, the more obvious the influence of the elastic modulus on the upwarp wavelength. This is because of the alteration in bending stiffness of the track slab due to changes in the elastic modulus, which leads to differing difficulties of bending deformation. When the track slab is subjected to an identical temperature rise load, the upwarp of the track slab with higher elastic modulus is more difficult, leading to a tendency for the deformation to extend longitudinally across the structure and dissipate energy over a larger upwarp range. Consequently, both the upwarp buckling critical temperature rise and the upwarp wavelength of the track slab increase as the elastic modulus rises.

Fig. 18 illustrates that under different initial upwarp amplitudes, the upwarp buckling critical temperature rise of the track slab increases linearly with the elastic modulus. Also, the impact of the elastic modulus on the critical temperature rise diminishes as the initial upwarp amplitude increases. Specifically, for every 1 GPa increase in the elastic modulus of the track slab, the critical temperature rise increases by approximately 0.3 ℃~2.3 ℃, indicating that increasing the elastic modulus is beneficial to the upwarp stability of the track slab.

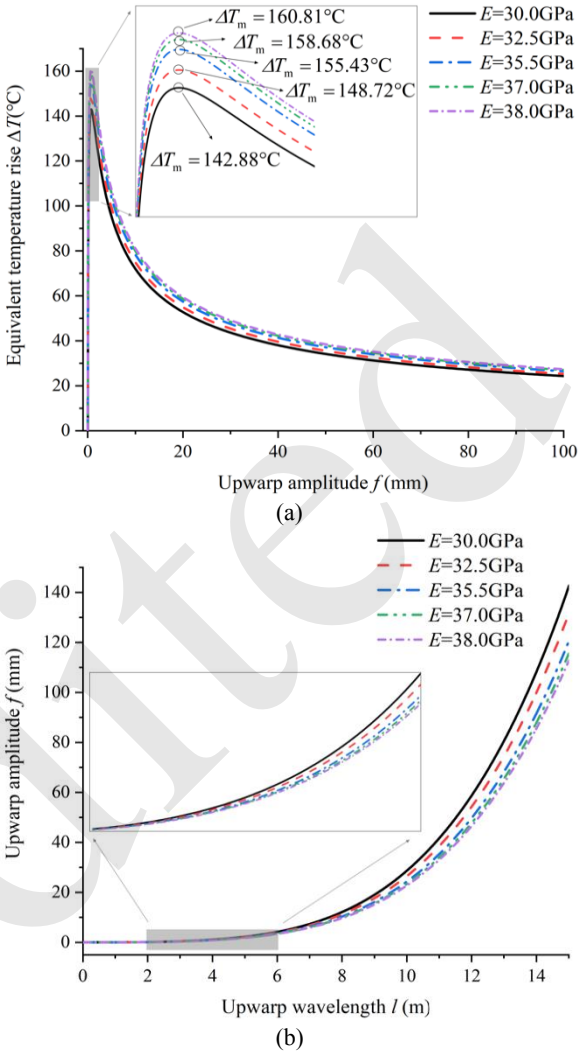

Fig. 17 Effect of elastic modulus on the upwarp buckling of the track slab: (a) upwarp buckling equilibrium path of the track slab; (b) variation of upwarp amplitude *f* with camber wavelength *l*

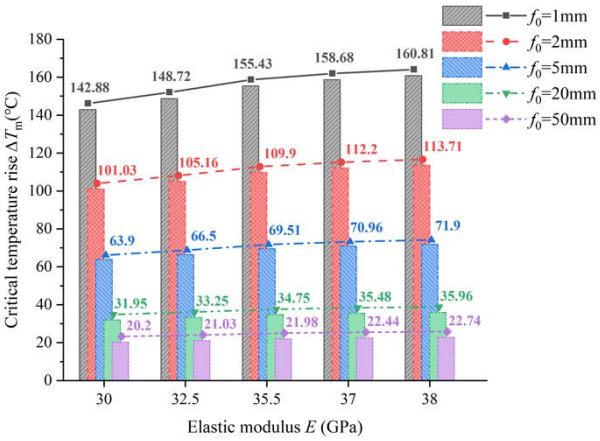

Fig. 18 Variation of ΔT_m with elastic modulus

4.5 The effect of the gravity load of the track slab

The upwarp of the track slab under the action of temperature load manifests as the displacement along the vertical direction of the structure. To realize the upwarp, it is necessary to first overcome the self-gravity field constraint that always exists in the deformation process, before and after the upwarp. In the ideal state, the per unit length gravity load q of the track slab is 12.75 kN/m. The per unit length gravity load is taken as 0.8q, 0.9q, 1.0q, 1.1q, and 1.2q, respectively, to study the influence of this factor on the upwarp buckling of the track slab.

The upwarp buckling equilibrium path of the track slab under different gravity loads is shown in Fig. 19(a). The results show that an increase in the gravity load of the track slab can significantly increase the upwarp buckling critical temperature rise, while the upwarp buckling critical amplitude is not sensitive to the change of the gravity load. This suggests that the gravity load does not alter the upwarp buckling mode of the track slab, but instead causes a synchronous 'scaling' of the upwarp equilibrium path. As shown in Fig. 19(b), the upwarp amplitude of the track slab increases with the increase of the gravity load at an identical upwarp wavelength, which is the opposite pattern of the influence of the elastic modulus on the *f*-*l* relationship. This is because the increase of gravity load not only increases the work done by gravity during the upwarping process, but also enhances the constraint effect at the end of the upwarp section, thereby restraining the longitudinal expansion of the upwarp. Relative to vertical deformation, the increase in gravity load more strongly inhibits the longitudinal expansion.

As shown in Fig. 20, the upwarp buckling critical temperature rise under different initial upwarp amplitudes exhibits a linear increase with the gravity load of the track slab. For every 0.1q change in the gravity load of the track slab, the upwarp buckling critical temperature rise changes by about 1.1 ℃~7.8 ℃. Relative to the impact of the elastic modulus of the track slab, alterations in the gravity load exert a more substantial effect on the vertical stability.

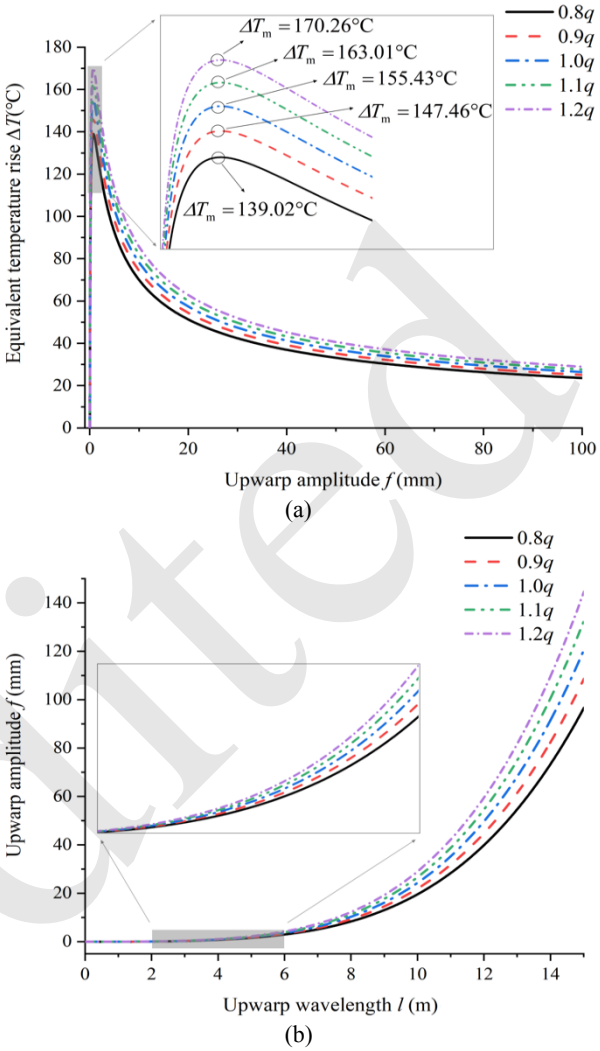

Fig. 19 Effect of q on the upwarp buckling of the track slab: (a) upwarp buckling equilibrium path of the track slab; (b) variation of upwarp amplitude f with camber wavelength l

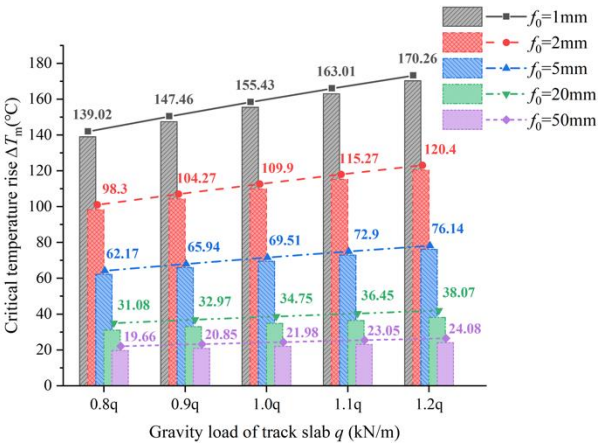

Fig. 20 Variation of ΔT_m with gravity load

4.6 The effect of track slab thickness

In the manufacturing process of track slabs, there will inevitably be some dimensional deviations. According to the manufacturing standard of the studied track slab, the allowable limit deviation for the thickness of prefabricated track slabs is set at +5 mm or -2 mm (State Railway Administration, 2015). Taking the initial upwarp curve of No.3 and f_0 = 1 mm as an example, the upwarp buckling development law of track slab is analyzed when h is 180 mm, 190 mm, 200 mm, 210 mm, and 220 mm, respectively.

As shown in Fig. 21(a), the development trend of the upwarp buckling equilibrium path for track slabs of various thicknesses remains consistent, with the post-buckling stage curves being almost parallel. Variations in slab thickness do not alter the development law of upwarp buckling. As the track slab thickness increases, so does the temperature rise required for a given upwarp amplitude, leading to a notable increase in both the upwarp buckling critical temperature rise and the final stable temperature rise. It can be seen from Fig. 21(b) that for an identical upwarp wavelength, the upwarp amplitude of the track slab gradually decreases with the increase of the track slab thickness. Under an identical temperature rise load, a thinner track slab tends to exhibit upwarp deformations characterized by longer upwarp wavelengths and larger upwarp amplitudes. This is because the increase of the track slab thickness will increase both the bending stiffness and gravity load of the section, resulting in different degrees of increase in the bending deformation energy and gravitational potential energy for different track slab thicknesses when reaching an identical upwarp amplitude.

The variation of the upwarp buckling critical temperature rise with the track slab thickness under different initial upwarp amplitudes is shown in Fig. 22. It is observed that ΔT_m increases linearly with the track slab thickness, and the variation law maintains a similar trend under different initial upwarp amplitudes. Specifically, for every 10 mm increase in the track slab thickness, the critical temperature rise increases by approximately 2.2°C~15.5°C. This indicates that the impact of track slab thickness on upwarp stability is more pronounced than the elastic modulus or gravity load of the track slab.

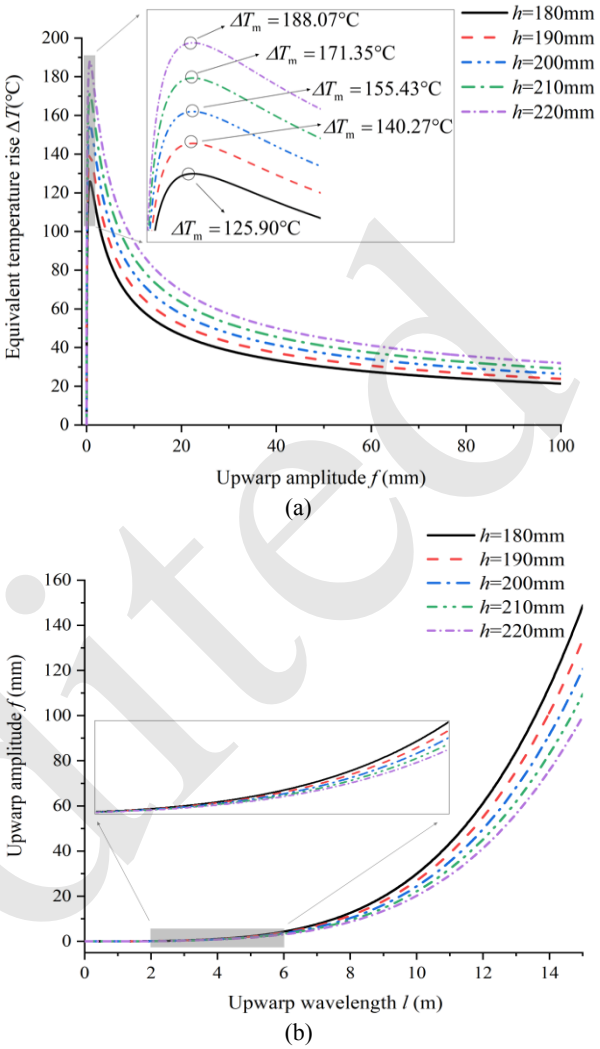

Fig. 21 Effect of h on the upwarp buckling of the track slab: (a) upwarp buckling equilibrium path of the track slab; (b) variation of upwarp amplitude *f* with camber wavelength *l*

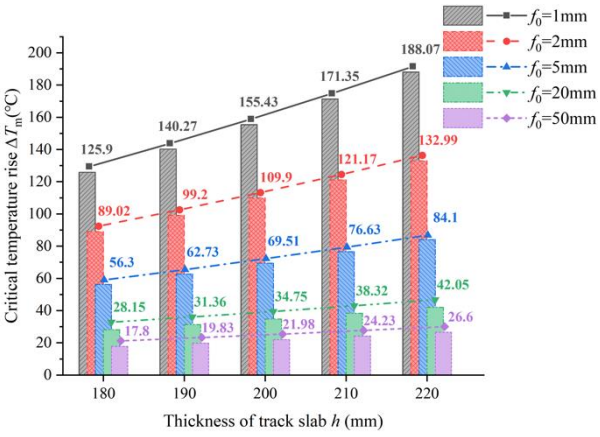

Fig. 22 Variation of ΔT_m with track slab thickness

5 Conclusions

This paper focused on the thermal-induced upwarp buckling of CRTS II ballastless track slabs under joint damage. Based on model tests and an energy method, the upwarp buckling behavior of the track slab was theoretically analyzed. The influence of initial upwarp amplitude, initial upwarp curve, elastic modulus, gravity load, and track slab thickness on the upwarp buckling of track slab was studied.

The upwarp buckling deformation characteristics of the track slab are intrinsically linked to its initial state. The upwarp deformation of the track slab in the narrow joint damage state is mainly concentrated in the joint damage position, and the upwarp buckling curve generally presents an inverted 'V' shape with concave ends.

The upwarp buckling development of the track slab undergoes three stages: stability, upwarp development, and post-buckling. Narrow joint defects will cause a significant decrease in the upwarp buckling critical temperature rise, and the track slab is more likely to produce local upwarp with larger deformation amplitude and shorter wavelength.

As the initial upwarp amplitude gradually increases, the upwarp buckling critical temperature rise of the track slab gradually decreases. Concurrently, the buckling mode transitions from 'sudden buckling' to 'progressive buckling' behavior. The initial upwarp amplitude is less than 6.5 mm, which ensures that the track slab does not undergo buckling.

The initial upwarp curve of the track slab has a negligible impact on the relationship between the upwarp amplitude f and the upwarp wavelength l. However, the upwarp buckling critical temperature rise of the track slab decreases as the boundary constraint of the initial upwarp curve intensifies.

The upwarp buckling critical temperature rise of the track slab changes linearly with the elastic modulus, gravity load, and thickness of the track slab. With the increase of the initial upwarp amplitude of the track slab, the influence of various factors on upwarp buckling critical temperature rise of the track slab becomes gradually weaker.

Acknowledgments

This work is supported by the National Natural Science Foundation of China (Nos. 52278459).

Author contributions

Chang XU designed the research and wrote the first draft of the manuscript. Tianci XU for the experimental setup. Weixing LIU and Zhixuan WANG processed the corresponding data. Pingrui ZHAO revised and edited the final version.

Conflict of interest

Chang XU, Tianci XU, Weixing LIU, Zhixuan WANG and Pingrui ZHAO declare that they have no conflict of interest.

References

Bouras Y, Vrcelj Z, 2020. Out-of-plane stability of concrete-filled steel tubular arches at elevated temperatures. *International Journal of Mechanical Sciences*, 187:105916. https://doi.org/10.1016/j.ijmecsci.2020.105916

Chen L, Chen JJ, Wang JX, et al., 2022. Effects of joint stiffness degradation on vertical stability of CRTS II slab ballastless track. *Construction and Building Materials*, 363:129812. https://doi.org/10.1016/j.conbuildmat.2022.129812

Cai XP, Luo BC, Zhong YL, et al., 2019. Arching mechanism of the slab joints in CRTS II slab track under high temperature conditions. *Engineering Failure Analysis*, 98:95-108. https://doi.org/10.1016/j.engfailanal.2019.01.076

Chen Z, Xiao JL, Liu XK, et al., 2018. Effects of initial up-warp deformation on the stability of the CRTS II slab track at high temperatures. *Journal of Zhejiang University-SCIENCE A (Applied Physics & Engineering)*, 19(12):939-950. https://doi.org/10.1631/jzus.A1800162

Dai GL, Ge H, 2020. Statistical analysis of the initial state characteristics of the longitudinally connected ballastless track on bridge. *Journal of Railway Engineering Society*, 37(09):1-6 (in Chinese).

He A, Liu Y, Sun XD, et al., 2024. A new elastic T-shape joint of longitudinally connected slab ballastless track structure for releasing thermal stress caused by non-uniform temperature loads. *Construction and Building Materials*, 416: 134997. https://doi.org/10.1016/j.conbuildmat.2024.134997

Huang YC, Gao L, Zhong YL, et al., 2021. Study on the damage evolution of the joint and the arching deformation of CRTS-II ballastless slab track under complex temperature loading. *Construction and Building Materials*, 309:125083. https://doi.org/10.1016/j.conbuildmat.2021.125083

Li H, Yang Z, Wen J, et al., 2023. Service life prediction of ballastless track concrete under the coupling effect of fatigue loads and environmental actions: a review. *Journal of Sustainable Cement-Based Materials*, 12(6):672-686. https://doi.org/10.1080/21650373.2022.2113172

Li Y, Chen J, Wang J, et al., 2021. Interfacial failure and arch-

ing of the CRTS II slab track reinforced by post-installed reinforcement bars due to thermal effects. *Engineering Failure Analysis*, 125:105405. https://doi.org/10.1016/j.engfailanal.2021.105405

Li Y, Li HY, Zhang GP, et al., 2023. Nonlinear responses of longitudinally coupled slab tracks exposed to extreme heat waves. *Engineering Structures*, 281:115789. https://doi.org/10.1016/j.engstruct.2023.115789

Liu P, Zheng Z, Yu Z, et al., 2020. Cooperative work of longitudinal slab ballast-less track prestressed concrete simply supported box girder under concrete creep and a temperature gradient. *Structures*, 27:559-569. https://doi.org/10.1016/j.istruc.2020.06.006

Liu XK, 2019. Study on upwarp stability of longitudinally coupled ballastless track under temperature pressure. PhD Thesis, Southwest Jiaotong University, Chengdu, China (in Chinese).

Liu XK, Liu XY, Xiao JL, et al., 2018. Vertical stability of longitudinal continuous ballastless track under temperature variation. *Journal of Southwest Jiaotong University*, 53(05):921-927 (in Chinese).

Liu XK, Zhang WH, Xiao JL, et al., 2019. Damage mechanism of broad-narrow joint of CRTS II slab track under temperature rise. *KSCE Journal of Civil Engineering*, 23(5):2126-2135. https://doi.org/10.1007/s12205-019-0272-2

Lou P, Shi T, 2023. Thermal arching and interfacial damage evolution of CRTS-II slab track under solar radiation in alpine and plateau regions. *Alexandria Engineering Journal*, 74:301-315. https://doi.org/10.1016/j.aej.2023.05.032

Ma ZR, Gao L, Liu X, et al., 2023. Slab arching degree identification and evaluation based on track dynamic inspection data. *Engineering Failure Analysis*, 155:107733. https://doi.org/10.1016/j.engfailanal.2023.107733

Matias S, Ferreira P, 2022. The role of railway traffic and extreme weather on slab track long-term performance. *Construction and Building Materials*, 322:126445. https://doi.org/10.1016/j.conbuildmat.2022.126445

MHURD (Ministry of Housing and Urban-Rural Development of the People's Republic of China), 2015. Code for Design of Concrete Structures, GB50010-2010. National Standards of the People's Republic of China (in Chinese).

Shi T, Sheng XW, Zheng WQ, et al., 2022. Vertical temperature gradients of concrete box girder caused by solar radiation in Sichuan-Tibet railway. *Journal of Zhejiang University-SCIENCE A (Applied Physics & Engineering)*, 23(5):375-387. https://doi.org/10.1631/jzus.A2100401

Song L, Liu H, Cui C, et al., 2019. Thermal deformation and interfacial separation of a CRTS II slab ballastless track multilayer structure used in high-speed railways based on meteorological data. *Construction and Building Materials*, 237:117528. https://doi.org/10.1016/j.conbuildmat.2019.117528

SRA (State Railway Administration), 2015. Concrete slab for CRTS II ballastless track, TB-T-3399-2015. Railway Industry Standards of the People's Republic of China (in Chinese).

Tang XY, Chen Z, Cai X, et al., 2023. Ballastless track arching recognition based on one-dimensional residual convolutional neural network and vehicle response. *Construction and Building Materials*, 408:133624. https://doi.org/10.1016/j.conbuildmat.2023.133624

Xu C, 2022. Study on upwarp stability of CRTS II Slab ballastless track under temperature load. Master Thesis, Southwest Jiaotong University, Chengdu, China (in Chinese).

Xu LY, Xu P, Xie J, 2021. The Effect of Mortar Bonding Softening on Thermal Buckling of Longitudinal Connected Track Slab. *Journal of Railway Engineering Society*, 38 (04):38-43 (in Chinese).

Xu YD, Yan DB, Zhu WJ, et al., 2020. Study on the mechanical performance and interface damage of CRTS II slab track with debonding repairment. *Construction and Building Materials*, 257:119600. https://doi.org/10.1016/j.conbuildmat.2020.119600

Yan DB, Xu YD, Zhu WJ, 2023. Effects of debonding repairment on interfacial damage and thermal deformation of CRTS II slab ballastless track. *Construction and Building Materials*, 389:131793. https://doi.org/10.1016/j.conbuildmat.2023.131793

Yang JB, Yang RS, Liu XY, et al., 2023. Upper Arch Stability Formula for CRTS II Track Slab Considering Joint Damage between Slabs. *Journal of the China Railway Society*, 45(09):133-141 (in Chinese).

Yang JB, Zeng Y, Liu XY, et al., 2015. Stability of CRTS II slab track based on energy norm. *Journal of Central South University (Science and Technology)*, 46(12):4707-4712 (in Chinese).

Zhao GT, Gao L, Zhao L, et al., 2017. Analysis of dynamic effect of gap under CRTS II track slab and operation evaluation. *Journal of the China Railway Society*, 39(01):1-10 (in Chinese).

Zhang Q, Cai XP, Zhong YL, et al., 2022. Temperature field and thermal effects of the longitudinal connected slab track based on the measurement data and thermal-fluid-structure coupling analysis. *Construction and Building Materials*, 343:128121. https://doi.org/10.1016/j.conbuildmat.2022.128121

Zhang SS, 2021. Interface damage mechanism between concrete layers under temperature loads. PhD Thesis, Gottfried Wilhelm Leibniz Universität Hannover, Lower Saxony, Germany.

Zhang XM, Liu JL, Zhu GM, et al., 2020. Stability Analysis and Uplift Treatment Study of Longitudinal Connected Slab Track. *Journal of Railway Engineering Society*, 37(03):21-26 (in Chinese).

Zhong YL, Gao L, Zhang YR, 2018. Effect of daily changing temperature on the curling behavior and interface stress of slab track in construction stage. *Construction and Building Materials*, 185:638-647.

https://doi.org/10.1016/j.conbuildmat.2018.06.224

Zhou R, Yin H, Li Y, et al., 2024. Mechanical performance analysis of double-block ballastless tracks in intercity railways under temperature and train loads. *Engineering Structures*, 315:118509. https://doi.org/10.1016/j.engstruct.2024.118509

Zhou R, Yue HH, Du YL, et al., 2023. Experimental and numerical study on interfacial thermal behaviour of CRTS II slab track under continuous high temperatures. *Engineering Structures*, 284:115964. https://doi.org/10.1016/j.engstruct.2023.115964

Zhou R, Zhu X, Huang JQ, et al., 2022. Structural damage analysis of CRTS Ⅱ slab track with various interface models under temperature combinations. *Engineering Failure Analysis*, 134:106029. https://doi.org/10.1016/j.engfailanal.2022.106029

中文概要

题　目：接缝损伤状态下的 CRTS II 型板式无砟轨道热致上拱屈曲分析

作　者：徐畅[1,2]，徐天赐[1,2]，刘卫星[1,2]，王志璇[1,2]，赵坪锐[1,2]

机　构：[1]西南交通大学，高速铁路线路工程教育部重点实验室，中国成都，610031；[2]西南交通大学，土木工程学院，中国成都，610031

目　的：在持续高温条件下，CRTS II 型轨道接缝部位极易损伤，轨道板存在上拱屈曲风险。本文旨在通过理论分析得到轨道板上拱屈曲平衡路径的解析公式，并探讨轨道板初始状态与结构参数（初拱幅值、初拱曲线型式、弹性模量、板厚和重力荷载等）对轨道板上拱屈曲响应的影响规律，以为轨道板上拱防治提供参考。

创新点：1. 开展模型试验，明确了轨道板上拱屈曲变形特征；2. 运用能量法原理，推导出轨道板上拱屈曲平衡路径的解析表达式。

方　法：1. 通过缩尺模型试验，得到轨道板在不同状态下的上拱屈曲变形曲线；2. 通过理论推导，建立了轨道板上拱幅值与温度荷载间的对应关系，验证理论方法的可行性和有效性；3. 通过参数分析，量化表征了轨道初始状态与结构参数对轨道板上拱屈曲的影响规律。

结　论：1.轨道板在窄接缝损伤状态下的上拱变形曲线大致呈现两端下凹的倒 V 形状；2. 轨道板上拱屈曲发展路径要经历稳定、上拱发展和后屈曲三个阶段，窄接缝缺损会导致上拱屈曲临界温升大幅下降；3.初拱幅值增大会导致轨道板上拱屈曲模式逐渐由“突跳屈曲”转变为“渐进屈曲”；4.轨道板上拱屈曲临界温升随初拱变形曲线边角约束的增强而减小；5. 轨道板上拱屈曲临界温升与弹性模量、重力荷载以及厚度间呈现线性关系。

关键词：CRTS II 型板式轨道；接缝损伤；上拱屈曲；形变能；温度荷载